HELSINKI INSTITUTE OF PHYSICS INTERNAL REPORT SERIES

Top-Quark Mass Measurement

Tuula Mäki

Helsinki Institute of Physics
P.O.Box 64, FI-00014 University of Helsinki, Finland

Dissertation for the degree of Doctor of Science in Technology to be presented with due permission of the Faculty of Information and Natural Sciences, Helsinki University of Technology, for public examination and debate in Auditorium K215 at Helsinki University of Technology (Espoo, Finland) on the 18th of March, 2008, at 12 o'clock noon.

ISBN 978-952-10-3714-6 (printed)
ISNB 978-952-10-3715-3 (PDF)
ISSN 1455-0563
Helsinki 2008
Yliopistopaino

Acknowledgements

This thesis is based on research work carried out as a member of the CDF Collaboration, with affiliation to Helsinki Institute of Physics and University of Helsinki.

I am grateful to professor Risto Orava for providing the opportunity to work at Fermilab. I believe it was an excellent chance to learn experimental particle physics. I am thankful for his encouragement, confidence in me, and always being available when needed. I would also like to thank him and Kenneth Österberg for providing suggestions how to improve my thesis, Barry Wicklund for checking the language of my thesis, and professor Rainer Salomaa for being the official supervisor of my thesis.

The top and top mass groups at CDF had an important role on my research, including help from several people. I am especially grateful to Jaroslav Antos, Andy Beretvas, Yen-Chu Chen and Roman Lysak for instructing my physics analyses. In addition, I want to thank all the CDF members who, in one way or another, contributed to my work, and the CDF silicon group for the experience I gained on detector operations.

My graduate studies were funded by GRASPANP graduate school and Helsinki Institute of Physics. Without the additional funding from Academy of Finland, Magnus Ehrnroothin säätiö, Teknillisen korkeakoulun tukisäätiö, and Waldemar von Frenckellin säätiö, I would not have been able to stay at Fermilab, and therefore it is gratefully acknowledged.

I had a great pleasure to make many friends at Fermilab. Without them, my years at Fermilab would not have been as enjoyable and memorable as they were.

Finally, I want to thank Mikko for his love, support and encouragement.

Tuula Mäki

Abstract

The top quark is the heaviest elementary particle. Its mass is one of the fundamental parameters of the standard model of particle physics, and an important input to precision electroweak tests.

This thesis describes three measurements of the top-quark mass in the dilepton decay channel. The dilepton events have two neutrinos in the final state; neutrinos are weakly interacting particles that cannot be detected with a multipurpose experiment. Therefore, the signal of dilepton events consists of a large amount of missing energy and momentum carried off by the neutrinos.

The top-quark mass is reconstructed for each event by assuming an additional constraint from a top mass independent distribution. Template distributions are constructed from simulated samples of signal and background events, and parametrized to form continuous probability density functions. The final top-quark mass is derived using a likelihood fit to compare the reconstructed top mass distribution from data to the parametrized templates. One of the analyses uses a novel technique to add top mass information from the observed number of events by including a cross-section-constraint in the likelihood function. All measurements use data samples collected by the CDF II detector.

Tiivistelmä

Top-kvarkki on raskain hiukkanen, jolla ei ole sisäistä rakennetta. Sen massa on yksi hiukkasfysiikan perusteorian, standardimallin, tärkeimmistä parametreista, ja lisäksi top-kvarkin massan avulla pystytään ennustamaan Higgsin bosonin massa.

Tämä väitöskirja käsittelee top-kvarkin massan mittaamista hajoamiskanavassa, jossa lopputila sisältää kaksi neutriinoa. Neutriinot vuorovaikuttavat hyvin heikosti materian kanssa, joten niitä ei voida järjestelmällisesti havaita hiukkasilmaisimilla. Näin ollen top-kvarkin massaa ei pystytä suoraan laskemaan tällaisten top-kvarkkikandidaattien mitatuista hajoamistuotteista.

Käyttämällä hyväksi muuttujaa, jonka jakauma ei riipu top-kvarkin massasta, jokaiselle valintakriteerit täyttävälle top-kvarkkikandidaatille pystytään arvioimaan massa. Puuttuvasta tiedosta ja mitattujen parametrien epätarkkuuksista johtuen saatu massajakauma ei piikity todellisen top-kvarkin massan kohdalle, joten mallinnetusta datasta luodaan mallijakaumat. Mitattu top-kvarkin massa saadaan vertaamalla datasta saatua jakaumaa mallijakaumiin. Yksi mittauksista yhdistää menetelmään top-kvarkkikandidaattien lukumäärästä saadun tiedon top-kvarkin massasta. Kaikki mittaukset käyttävät CDF-kokeen mittaamaa dataa.

List of Publications

I Measurement of the top quark mass using template methods on dilepton events in $p\bar{p}$ collisions at $\sqrt{s}$=1.96 TeV, A. Abulencia *et al.* with T. Maki (CDF Collaboration), Phys. Rev. D **73**, 112006 (2006).

II Top-Quark Mass Measurement from Dilepton Events at CDF II, A. Abulencia *et al.* with T. Maki (CDF Collaboration), Phys. Rev. Lett. **96**, 152002 (2006).

III Cross-Section-Constrained Top-Quark Mass Measurement from Dilepton Events at the Tevatron, T. Aaltonen *et al.* with T. Maki (CDF Collaboration), Phys. Rev. Lett. **100**, 062005 (2008).

IV Status and performance of the CDF Run II silicon detector, T. Maki on behalf of the CDF Collaboration, Nucl. Instrum. Methods A **579**, 723-725 (2007).

V Measurement of the Top Quark Mass in the Dilepton Channel at CDF and DØ , T. Mäki on behalf of the CDF and DØ Collaborations, Particles and Nuclei International Conference, Editors Peter D. Barnes *et al.*, AIP conference proceedings **842** 625-627 (2006). ISBN 0-7354-0338-4.

VI Top quark mass measurements at CDF, T. Maki on behalf of the CDF Collaboration, The 2007 Europhysics Conference on High Energy Physics, Editor Roger Barlow, accepted for publication in Journal of Physics: Conference Series.

Publication I: Measurement of the top quark mass using template methods on dilepton events in $p\bar{p}$ collisions at $\sqrt{s}$=1.96 TeV

A. Abulencia *et al.* with T. Maki (CDF Collaboration)

Physical Review D **73**, 112006 (2006)

The top quark is the heaviest elementary particle. Its mass is of principal interest both as a fundamental parameter of the standard model of particle physics and as an important input to precision electroweak tests. This publication describes three template top mass analyses in the dilepton channel, and the combination of the results.

The author of this thesis was one of the two corresponding authors for the Full Kinematic Analysis (KIN), participated in the correlation studies for the combination, and contributed to the writing of the paper.

Publication II: Top-Quark Mass Measurement from Dilepton Events at CDF II

A. Abulencia *et al.* with T. Maki (CDF Collaboration)

Physical Review Letters **96**, 152002 (2006)

This paper describes a top-quark mass measurement in the dilepton channel using a matrix element method, and the combination of all four top mass measurements in the dilepton channel using the same data set.

The author of this thesis was one of the two corresponding authors for the KIN analysis, and participated in the correlation studies for the combination.

Publication III: Cross-Section-Constrained Top-Quark Mass Measurement from Dilepton Events at the Tevatron

T. Aaltonen *et al.* with T. Maki (CDF Collaboration)

Physical Review Letters **100**, 062005 (2008)

This publication describes the first top-quark mass measurement which uses a cross-section-constraint. This novel technique combines the top mass

information from the reconstructed top mass distribution and the observed number of events. In addition, the analysis was significantly improved by dividing the event sample into two subsamples with different purities. The result represented the single most precise top-quark mass measurement in the dilepton channel.

The author of this thesis carried out the analysis independently and wrote the paper.

Publication IV: Status and performance of the CDF Run II silicon detector

T. Maki on behalf of the CDF Collaboration

Nuclear Instruments Methods in Physics Research Section A **579**, 723-725 (2007)

The improvement on the top-quark mass measurement from dividing the sample into two subsamples, described in the Publication III, was achieved by utilizing "b-tagging". The b-tagging is based on the data measured with the silicon detector. This paper describes the performance and longevity studies of the silicon detector.

The author was part of the operations group of the CDF Run II silicon detector, was one of the on-call experts, studied and predicted the signal-to-noise ratios described in the paper, and wrote the paper.

Publication V: Measurement of the Top Quark Mass in the Dilepton Channel at CDF and DØ

T. Mäki on behalf of the CDF and DØ Collaborations

Particles and Nuclei International Conference, Editors Peter D. Barnes *et al.*, AIP conference proceedings **842** 625-627 (2006). ISBN 0-7354-0338-4

This conference contribution summarizes the preliminary CDF and DØ top-quark mass measurements in the dilepton channel from summer 2005.

The author of this thesis was one of the two corresponding authors for

the KIN analysis, presented the CDF and DØ results at the conference, and wrote the paper.

Publication VI: Top quark mass measurements at CDF

T. Maki on behalf of the CDF Collaboration

The 2007 Europhysics Conference on High Energy Physics, Editor Roger Barlow, accepted for publication in Journal of Physics: Conference Series

This paper reports the latest top-quark mass measurements from the CDF experiment.

The author of this thesis independently carried out the template and cross-section-constrained top mass measurements in the dilepton channel, presented the CDF top-quark mass measurements at the conference, and wrote the paper.

Contents

1 Introduction

The discovery of the top quark in 1995 was a major triumph of the standard model of particle physics. It marked the culmination of nearly two decades of intense research at accelerators around the world. The discovery completed the three-generation structure of the standard model.

The most striking feature of the top quark is its mass. It is about 35 times heavier than the next heaviest quark, and it is the heaviest known elementary particle. Because the top quark is so heavy, it has an extremely short lifetime. Unlike other quarks, the top quark decays before it can combine with virtual quarks and antiquarks to form top-flavored hadrons. Therefore, the top quark is the only quark that decays before the process of hadronization.

The top-quark mass is one of the most important parameters of the standard model. Along with Higgs- and W-boson masses, it contributes to radiative corrections in theoretical calculations of many observables that have been measured with good precision. Therefore, precision measurement of the top mass helps constrain the mass of the standard model Higgs boson. The large mass of the top quark takes on even greater significance in various extensions of the standard model.

It is important to measure the top-quark mass in all decay channels because any discrepancy among the measured top masses in different decay channels could indicate the presence of non-standard model events in the samples. The publications presented in this thesis describe experimental measurements of the top-quark mass in a decay channel which has two neutrinos in the final state.

Because neutrinos cannot be detected with a general purpose detector, the signal of such a top decay consists of a large amount of missing energy and momentum. With an additional constraint, the top-quark mass is reconstructed for each event, and the resulting distribution of reconstructed top masses is compared to model distributions.

The measurements utilize data samples collected by the CDF II detector. The CDF II detector is one of the two multipurpose experiments at the proton-antiproton Tevatron collider, which is currently the highest-energy particle accelerator in the world. It is located at Fermi National Accelerator Laboratory in Illinois, USA.

2 Standard Model of Particle Physics

The standard model (SM) is the theory describing the basic phenomena in elementary particle physics. It contains all the known fundamental particles and three of the known interactions: strong, electromagnetic, and weak interactions. Only gravity is not included in the SM [1].

Within the SM, there are two kinds of matter particles: quarks and leptons [1]. They form three families, each consisting of two quarks and two leptons. The vast majority of stable matter is made up of particles in the first family. The other two families are similar to the first family, except that the particles are more massive and unstable.

The interactions are mediated by gauge bosons [1]. The gauge bosons of the electromagnetic and strong interactions, photons and gluons, are massless particles. The weak interaction is mediated by the massive vector bosons, $W^{\pm}$ and Z^0. In local gauge invariant theories, where the observed physical quantities do not depend on a particular choice of the potential used to describe the fields, gauge bosons should be massless. In the SM this is solved, still preserving the gauge invariance, by introducing a spontaneous symmetry breaking.

This symmetry breaking is called the Higgs mechanism [1]. In the Higgs mechanism, the scalar Higgs field imparts masses to the vector bosons ($W^{\pm}, Z^0$) and creates one massive neutral scalar boson (H). This scalar boson is called the Higgs boson and its mass is a free parameter of the SM. The fermion masses can be explained by the Yukawa coupling of the Higgs boson to the fermions. The Higgs boson has not yet been found experimentally, and search for it remains one of the most important tasks for the field of particle physics.

2.1 Top Quark

The top quark was observed at Fermilab in 1995 by the CDF and DØ Collaborations [2, 3]. As all other quarks and leptons have a same family partner, the existence of the top quark was anticipated since the discovery of the bottom quark in 1977 [4, 5]. The experimental discovery of the top quark took much longer than originally anticipated because the top quark was not ex-

pected to be so heavy. The current world average of the measured top-quark mass is about 171 GeV/c^2 [6].

At hadron colliders, the top quarks can be produced via the strong or electroweak interaction [7]. At the Tevatron center-of-mass energy, $\sqrt{s}$=1.96 TeV, the strong interaction production is dominant, and it results in a pair of top and antitop quarks ($t\bar{t}$). The $t\bar{t}$ production at the Tevatron can be described by perturbative QCD [8]. In this approach, a hard scattering process between proton and antiproton is the result of an interaction between quarks and gluons, which are constituents of the incoming hadrons. The total production cross section for $p\bar{p} \to t\bar{t}$ can be calculated as

$$\sigma(p\bar{p} \to t\bar{t}) = \Sigma_{a,b} \int dx_a dx_b f_a^p(x_a, \mu^2) f_b^{\bar{p}}(x_b, \mu^2) \widehat{\sigma}^{ab \to t\bar{t}}(\widehat{s}, \mu^2, M_t), \qquad (1)$$

where the summation indices a and b run over light quarks and gluons. This formula expresses the total cross section in terms of the parton-parton process $ab \to t\bar{t}$, where a and b are partons contained in the initial proton and antiproton carrying momentum fractions of x_a and x_b. The parton distribution functions f_a^p and $f_b^{\bar{p}}$ are the probability densities of finding a parton with a given momentum fraction in a proton or antiproton, and $\widehat{\sigma}$ is the subprocess cross section at a parton-parton center-of-mass energy of $\widehat{s} = x_a x_b s$. The renormalization and factorization scales, here chosen to be the same value μ, are arbitrary parameters. The first is introduced by the renormalization procedure, and the second by the splitting of the total cross section into perturbative ($\widehat{\sigma}$) and non-perturbative ($f^p, f^{\bar{p}}$) parts. The dependence of observables on μ is an artifact of truncating the perturbation expansion at finite order. If the calculations could be performed to all orders, the dependence on μ would vanish.

Since there has to be at least enough energy to produce a $t\bar{t}$ pair at rest, $\widehat{s} \geq 4M_t^2$. Therefore, $x_a x_b = \widehat{s}/s \geq 4M_t^2/s$. Because the probability of finding a quark of momentum fraction x in the (anti)proton falls off with increasing x (see Fig. 1), the typical value of $x_a x_b$ is near the threshold for $t\bar{t}$ production. By setting $x_a \simeq x_b = x$, we obtain

$$x \simeq \frac{2M_t}{\sqrt{s}} \simeq 0.17 \qquad (2)$$

as the typical value of x for $t\bar{t}$ production at the Tevatron. With this value of x, the u- and d-valence quark distribution functions are larger than the

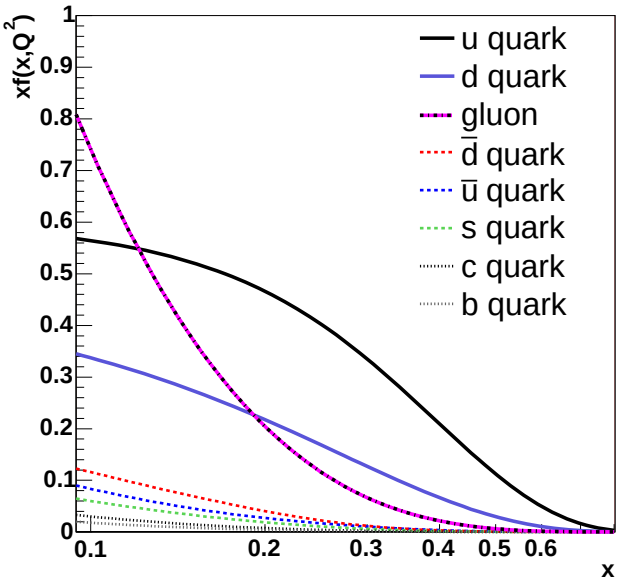

Figure 1: CTEQ5L parton distribution functions $xf(x, Q^2)$ with $Q^2 = (175\ \text{GeV})^2$ [9]. Q^2 marks the energy scale and x is the momentum fraction.

gluon distribution function. This explains why quark-antiquark annihilation dominates at the Tevatron, being about 85% of $t\bar{t}$ production. The leading order Feynman diagrams for $t\bar{t}$ production are shown in Fig. 2.

The theoretical calculation of the $t\bar{t}$ production cross section gives $\sigma_{t\bar{t}}$= $6.7^{+0.7}_{-0.9}$ pb for M_t=175 GeV/c^2 [10]. The production via the electroweak interaction results in a single top quark (see Fig. 3), and its theoretical cross section is 2.9±0.4 pb [11, 12]. Due to the similarity of the single top signature to other physics processes, it has not yet been observed in 5σ level, though there is 3.4σ evidence for it [13]. Compared to the total production of events, top quarks are relatively rare at the Tevatron: the total cross section is about 10^{10} higher than the $t\bar{t}$ cross section [14].

The top quark is by far the heaviest of the fundamental particles. Its mass is 10000 times larger than the lightest of the quarks, and 35 times larger than the second heaviest quark, the bottom quark. Due to the large mass of the

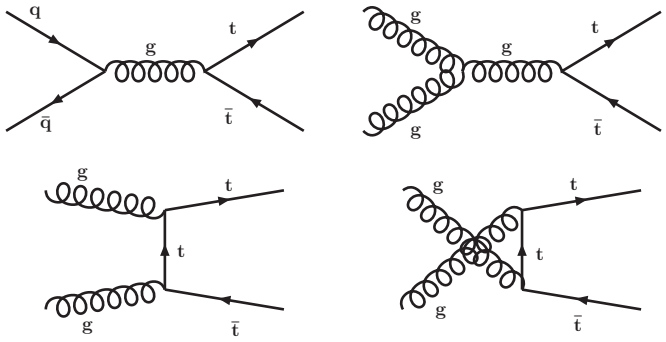

Figure 2: Leading order Feynman diagrams for $t\bar{t}$ production.

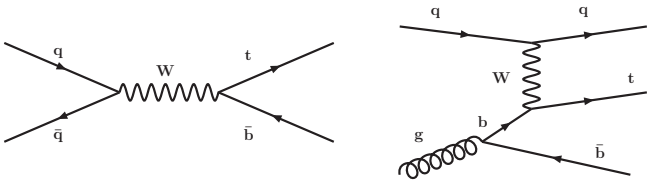

Figure 3: Representative Feynman diagrams for single top production.

top quark, the top mean lifetime is only $\tau_t \sim 10^{-25}$ s. This timescale is shorter than the timescale required for hadronization, $\tau_{had} \sim 10^{-24}$ s [15], a process in which a quark combines with quarks and antiquarks spontaneously created from the vacuum to form hadrons. Therefore, the top quark decays before it hadronizes, and its momentum and spin are transfered to its decay products. It is the only quark which decays before hadronization.

Top decay products span the entire spectrum of quarks and leptons [16]. Within the SM, the top quark decays almost exclusively into a W boson and a b quark. The W boson decays almost instantaneously either leptonically into a charged lepton - neutrino pair or hadronically into a quark - antiquark pair. Since there are two top quarks in each $t\bar{t}$ event and the W bosons decay independently, the $t\bar{t}$ events can be classified into three categories according to the W boson decays: dilepton, lepton+jets, and all-hadronic decay channel.

- In the all-hadronic channel both W bosons decay into a quark - an-

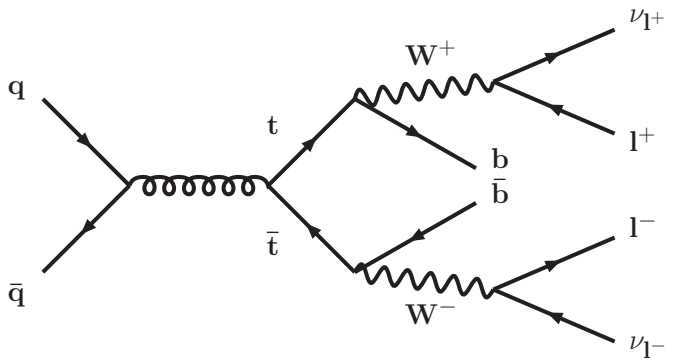

Figure 4: Feynman diagram of dilepton $t\bar{t}$ event.

tiquark pair. The branching ratio for this decay mode is 44%, but it suffers from a large QCD background.

- In the lepton+jets channel one W boson decays hadronically, and the other decays leptonically into $e\nu_e$ or $\mu\nu_\mu$. This channel has a branching ratio of 30%, and a managable background.
- In the dilepton channel both W bosons decay leptonically into $e\nu_e$ or $\mu\nu_\mu$. These events have a very low background, but only 5% branching ratio. A Feynman diagram of a dilepton $t\bar{t}$ event is shown in Fig. 4. This thesis describes analyses in the dilepton channel.

The remaining 21% of $t\bar{t}$ decays involve τ leptons, which are difficult to identify and therefore usually not considered in experimental measurements.

2.2 Top-Quark Mass

The top-quark mass is a fundamental parameter in the SM. It plays a key role in predictions of many SM observables by contributing to their radiative corrections [17]. A good example is the W-boson propagator, illustrated in Fig. 5. This kind of diagram can exist for any type of quark or lepton, but the very large mass of the top quark makes the top quark contribution dominant.

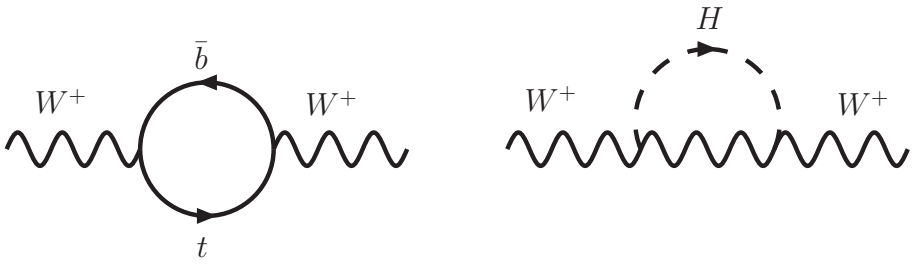

Figure 5: Loop diagrams generating corrections to the theoretical W-boson mass. On the left is a fermion loop with the top and b quarks. On the right is a Higgs-boson loop.

By defining the electroweak mixing angle θ_W by

$$\sin^2\theta_W = 1 - \frac{M_W^2}{M_Z^2}, \tag{3}$$

the theoretical W-boson mass can be written as:

$$M_W^2 = \frac{\pi\alpha}{\sqrt{2}G_F \sin^2\theta_W(1-\Delta r)}, \tag{4}$$

where α is the fine structure constant, G_F the Fermi constant, and the one loop radiative corrections from the top quark can be approximated as

$$\Delta r_{top} = \frac{3G_F M_t^2}{8\sqrt{2}\pi^2 \tan^2\theta_W}. \tag{5}$$

Because the uncertainty on M_t is about an order of magnitude higher than the other uncertainties, and it contributes quadratically, the precision of the theoretical M_W prediction is currently limited by the precision of M_t.

The Higgs-boson loops introduce similar corrections to the theoretical prediction of M_W, see Fig. 5. The one loop radiative corrections calculated from the Higgs boson are

$$\Delta r_{Higgs} \simeq \frac{3G_F M_W^2}{8\sqrt{2}\pi^2}(\ln\frac{M_H^2}{M_Z^2} - \frac{5}{6}). \tag{6}$$

Therefore, by combining the information from the experimental measurements of the top-quark and the W-boson masses and the radiative corrections, the SM Higgs-boson mass can be predicted. Until the Higgs boson is observed experimentally, this information can be used to guide experimental searches. Once the Higgs boson is observed, the top-quark and W-boson masses can be used to check the consistency of the SM. If the observed Higgs mass were not consistent with the prediction calculated from the top-quark and W-boson masses, this would indicate that the basic matter and forces are not fully described by the SM. Figure 6 shows the electroweak constraints on the SM Higgs-boson mass using the current world averages of the top-quark mass measurement, $M_t = 170.9 \pm 1.8$ GeV/c^2 [6], and the W-boson mass measurement, $M_t = 80.398 \pm 25$ GeV/c^2 [17].

The large mass of the top quark takes on an even greater significance in various extensions of the SM [18]. With precise knowledge of the top-quark mass, these theories can be tuned or even excluded. In addition, the Yukawa coupling of the top quark to a SM Higgs boson is roughly unity, possibly indicating a special role for the top quark in the electroweak symmetry breaking [19].

2.2.1 Top-Quark Mass Measurement in the Dilepton Channel

The top-quark mass measurement from the dilepton events provides different advantages and challenges compared to the other decay channels. The advantages of the dilepton events for the top mass reconstruction include that the dilepton events have the highest signal-to-background ratio because of the unique signature, and that they have the smallest number of combinatoric matches between measured particles and top decay products. For example, there are up to 90 possible ways to assign the measured particles to the parton-level decay products in the all-hadronic channel, whereas there are only two possible ways in the dilepton channel.

The typical distance scale of hadronization is about 1 fm. It is about an order of magnitude larger than a typical vertex separation of the two W boson decays in a $t\bar{t}$ event. Therefore, the colored particles from $t\bar{t}$ decay may interact before hadronization and, in principle, make it impossible to subdivide the hadronic final states into two groups of particles. This effect is called color reconnection [21]. Because the dilepton events have only two

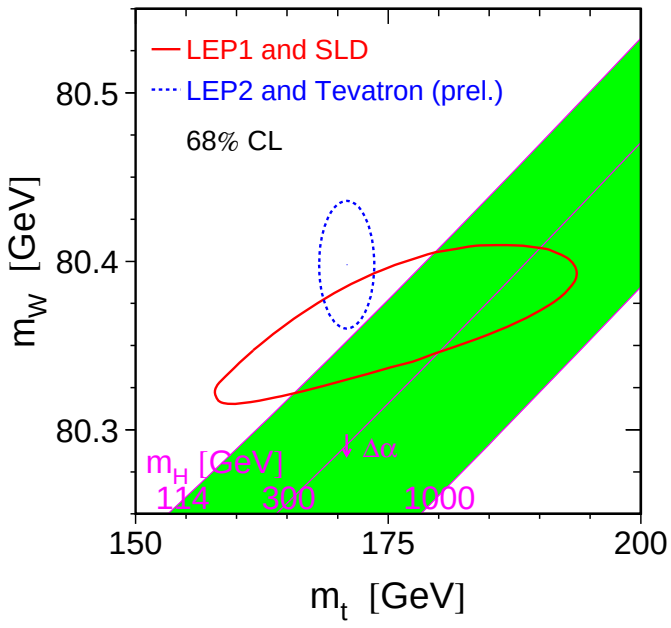

Figure 6: Electroweak constraints on the Higgs-boson mass as a function of the top-quark and W-boson masses [17]. The dotted curve shows the experimental measurements of the top-quark and W-boson masses, the continous curve shows the indirect measurement from precision electroweak data.

quarks in the final state, compared to four in the lepton+jets and six in the all-hadronic channels, the dilepton channel is least sensitive among the $t\bar{t}$ decay channels to color reconnections and their uncertainties.

The mass reconstruction from dilepton events is challenging because both neutrinos escape detection and also because the dilepton channel has the smallest branching ratio. In the lepton+jets and all-hadronic channels, which have hadronically decaying W bosons, it is possible to transfer the main systematic uncertainty into a statistical uncertainty by using the known W-boson mass to calibrate the energies of the jets from the W-boson decays. This calibration is not possible in the dilepton channel, and therefore the current measurements in the dilepton channel have larger systematic uncer-

tainties than the measurements in the other decay channels.

Traditionally, the lepton+jets channel has offered the most precise measurements of the top-quark mass. However, measuring the top mass precisely in the dilepton channel is important because it provides an independent measurement of M_t. First, the top mass from dilepton events can be compared to measurements from other decay channels. Because all top mass measurements assume a sample composition of $t\bar{t}$ and SM background events, the measured top masses from different channels should be consistent. A discrepancy between measured masses could indicate, for example, the presence of non-SM events in the samples [20], or inadequate modeling of the experimental quantities or the theoretical distributions, including color reconnection effects. Second, if the measurements from different decay channels are consistent within uncertainties, then they can be combined, and the top mass measurement from the dilepton channel can improve the overall precision of the top mass measurement.

3 Accelerator and Experiment

The Fermi National Accelerator Laboratory (Fermilab) is one of the main particle physics facilities in the world. It operates the proton-antiproton Tevatron Collider, which is currently the highest-energy collider in the world. The top quark was discovered at Fermilab with Tevatron collisions in 1995, and it still remains the only place where top quarks have been produced.

3.1 Collider

The accelerator complex, shown in Fig. 7, consists of several components that are used to produce, store, accelerate, and collide the protons and antiprotons at a center-of-mass energy of $\sqrt{s}$=1.96 TeV.

The proton acceleration begins with hydrogen gas in the Cockcroft-Walton pre-accelerator. The hydrogen gas is ionized to create H^- ions, which are then accelerated to 750 keV. The ions are sent to the Linac, a 150 m long linear accelerator which accelerates the ions to 400 MeV.

Next the ions pass through a carbon foil, which removes the electrons, leaving only the positively charged protons. The protons are directed to a circular accelerator, the Booster, which accelerates the protons to 8 GeV. In the Main Injector, the protons can be accelerated to 150 GeV and injected to Tevatron, or they can be accelerated to 120 GeV and used for antiproton production.

Antiprotons are produced by colliding a beam of 120 GeV protons to a nickel foil. The collisions produce a wide range of secondary particles, including antiprotons. The antiprotons are collected, focused and stored in the Accumulator ring. When a sufficient number of antiprotons has been produced, they are sent to the Main Injector for acceleration and injection into the Tevatron.

The Tevatron is a 6 km circumference proton-antiproton synchrotron collider. It receives 150 GeV protons and antiprotons from the Main Injector, and accelerates them to 980 GeV. The protons and antiprotons circulate in opposite directions in the same beam pipe. They are both arranged into 36 bunches which form 3 trains of 12 bunches each. At a luminosity of

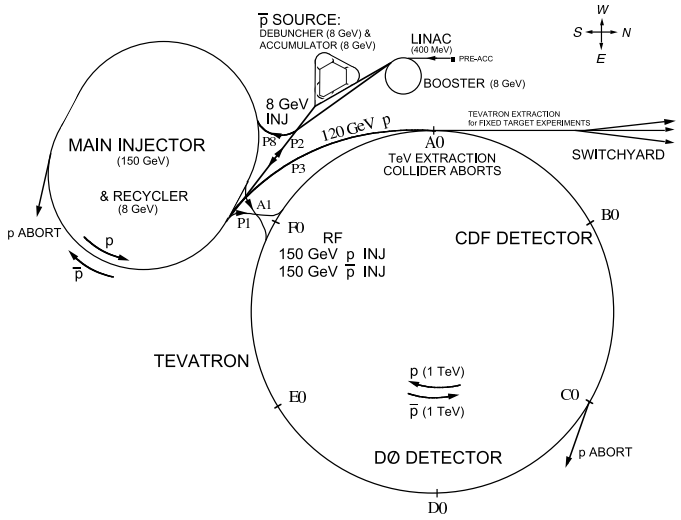

Figure 7: Schematic view of the accelerator chain.

10^{32} cm^{-2}s^{-1}, there are approximately 10^{12} protons per bunch and about an order of magnitude fewer antiprotons per bunch. The bunches are brought into collision in the centers of the CDF and DØ detectors.

The Tevatron collider will remain the highest-energy particle accelerator until the start of the Large Hadron Collider (LHC) in 2008. The LHC will collide protons on protons with a center-of-mass energy of 14 TeV, and with a design luminosity 100 times higher than Tevatron. The main physics processes at the LHC, and most of the challenges to collect and interpret the data are similar to those at the Tevatron.

3.2 CDF Experiment

The CDF II detector, shown in Fig. 8, is a multipurpose detector [22, 23]. It is made up of three fundamental sections: tracking detectors, calorimeters, and muon detectors.

The tracking detectors include the silicon microstrip detectors and the central outer tracker. They are located inside a 1.4 T magnetic field created by a superconducting solenoid. Due to the magnetic field, the transverse

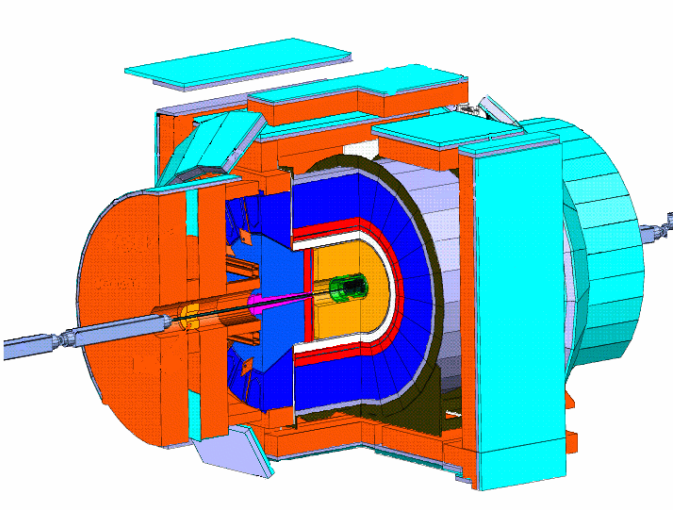

Figure 8: A graphical view of the CDF detector.

momentum of a charged particle can be determined by measuring the radius of curvature of the track.

The CDF calorimeters are scintillator sampling calorimeters. A sampling calorimeter alternates layers of an absorber material with an active material. When a particle passes through the absorber layers, it showers and deposits energy in both the absorber and the active material. The total energy read out from all the sampling layers is proportional to the energy of the incident particle(s).

The muon chambers are drift chambers interleaved with steel absorber plates outside the calorimeters. Since ionization is the dominant energy loss mechanism for muons, they leave only a small amount of energy in the calorimeters before they traverse the muon chambers. Nearly all other detectable particles are absorbed in the calorimeters and the steel absorber plates.

The collision rate at CDF is 2.5 MHz, which is too high to allow the recording of every event. Physically interesting events are chosen using a three level trigger system, each level putting more stringent selection criteria on the event. The first two levels are made of custom built hardware, while the third level consists of a farm of PCs. The trigger system reduces the

event output rate to a recordable 75 Hz.

CDF employs cylindrical coordinates where θ and ϕ are the polar and azimuthal angles with respect to the proton beam. Transverse energy and momentum are defined as $E_T = E \sin\theta$ and $p_T = p \sin\theta$, where E is the energy and p is the momentum. The missing transverse energy vector $\vec{\not\!\!E}_T$ is defined by

$$\vec{\not\!\!E}_T = -\sum_i E_T^i \hat{n}_i, \ i = \text{calorimeter tower number with } |\eta| < 3.6, \qquad (7)$$

where $\hat{n}_i$ is a unit vector perpendicular to the beam axis and pointing at the ith calorimeter tower, and η is the pseudorapidity. The quantity $\not\!\!E_T$ is defined as $\not\!\!E_T = |\vec{\not\!\!E}_T|$.

4 Top-Quark Mass Measurement

This thesis includes three top mass measurements in the dilepton channel. All the measurements use a technique called "template method" that reconstructs a top-quark mass, m_t^{rec}, for each event and compares the distribution of m_t^{rec} with template distributions derived from simulation. The first measurement is a template top mass measurement using a data sample of 30 events corresponding to 0.34 fb^{-1}. It is described in detail in Publications I and V. This measurement was combined with other top mass measurements in the dilepton channel as described in Publication II. The second measurement is a significantly improved version of the first one. This enhanced version treats b-tagged and non-tagged events separately, has an optimal mass reconstruction probability requirement, and uses a data sample of 70 events corresponding to 1.2 fb^{-1}. The third measurement adds a cross-section-constraint to the second method to reduce the statistical uncertainty further by 20%. The second and the third measurements are described in this section, as well as in Publications III and VI.

4.1 Event Selection

Because of the extremely short lifetime of the top quark, it is detected by measuring its daughter particles. Although the much lighter decay products have good angular separation and high transverse momenta, the reconstruction of the daughter particles involves several challenges:

- Electrons form compact showers in the calorimeter and have associated tracks in the central tracking volume of the detector.
- Muons are highly penetrating particles. They are distinguished by their hit patterns in the muon detectors, matched tracks in the central tracker, and small energy depositions in the calorimeters.
- Neutrinos are weakly interacting particles which escape the detector. Partial information on their momenta can be obtained from the missing transverse energy vector $\vec{\not\!\!E}_T$.
- b quarks hadronize and form jets of multiple charged particles. Jets deposit broad distributions of energy in the electromagnetic and hadronic

calorimeters. Jets are reconstructed based on clusters of calorimeter energy; the energy resolution on jets is less precise than that for charged leptons.

The signature of a dilepton $t\bar{t}$ event consists of two high-momentum leptons, missing transverse energy ($\not\!\!E_T$) from the neutrinos, two jets from the b-quarks, and possibly additional jets produced by initial or final state radiation. The event sample was collected using an inclusive lepton trigger that required an electron with $E_T > 18$ GeV or a muon with $p_T > 18$ GeV/c. After offline reconstruction, we selected events with

- Two leptons with $p_T > 20$ GeV/c. At least one of the leptons was required to be isolated.
- $\not\!\!E_T \geq 25$ GeV
- At least two jets with $E_T \geq 15$ GeV

The main sources of backgrounds are diboson production ($q\bar{q} \rightarrow Z/\gamma^*/W \rightarrow WW/WZ/ZZ$), Drell-Yan dilepton production ($q\bar{q} \rightarrow Z/\gamma^* \rightarrow e^+e^-/\mu^+\mu^-/\tau^+\tau^-$), and $W \rightarrow l\nu$+jets events where a jet "fakes" the signature of the second lepton. Additional selection requirements were introduced to reduce the background [24]. The expected and observed numbers of events in the 1.2 fb^{-1} data sample are shown in Table 1.

The sensitivity of the top mass measurement can be improved by dividing the sample into two subsamples with significantly different signal-to-background ratios. Since the $t\bar{t}$ events have two b quarks and the background events usually do not have b quarks, a subsample with higher signal purity can be selected by detecting b quarks. A b quark immidiately hadronizes, but typically travels about 0.5 cm from the primary interaction vertex before decaying into a jet containing multiple charged particles. Such a displaced, secondary vertex can be reconstructed using data from a good vertex detector, like the CDF silicon detector. Stable operation and efficient performance of the CDF silicon detector, which is described in Publication IV, is crucial for reliable b-tagging at CDF.

The first subsample includes the events in which at least one of the jets is b-tagged. This b-tagged subsample has an expected signal-to-background

ratio of 11:1. The non-tagged sample comprises of the events in which none of the jets is identified as a b-quark candidate. The expected and observed number of events in each subsample are shown in Table 2.

Table 1: Expected and observed numbers of events passing the event selection criteria (1.2 fb^{-1} event sample).

	Expected background
diboson	5.8 ± 0.9
$W\gamma$	0.1 ± 0.1
$Z/\gamma^* \to ll, l = e, \mu, \tau$	10.9 ± 2.3
fakes	8.8 ± 3.9
Total	25.6 ± 5.5
	Expected signal
$t\bar{t}$ ($M_t = 170$ GeV/c^2)	62.1 ± 4.3
Total expected	87.7 ± 8.9
Data	77

Table 2: Expected and observed number of events in each subsample (1.2 fb^{-1} event sample).

	b-tagged	non-tagged
Expected background	2.8±1.1	22.8±5.0
Expected signal ($M_t = 170$ GeV/c^2)	33.6±2.5	28.5±2.1
Data	32	45

4.2 Template Top Mass Measurement

4.2.1 Per-event Mass Reconstruction

The top mass reconstruction is initiated by writing the kinematic equations for the dilepton $t\bar{t}$ decay:

$$\begin{array}{rcl} \vec{p}_b + \vec{p}_{W^+} & = & \vec{p}_t \\ \vec{p}_{\bar{b}} + \vec{p}_{W^-} & = & \vec{p}_{\bar{t}} \\ \vec{p}_{l^+} + \vec{p}_\nu & = & \vec{p}_{W^+} \\ \vec{p}_{l^-} + \vec{p}_{\bar{\nu}} & = & \vec{p}_{W^-} \\ M_t & = & M_{\bar{t}} \\ M_{W^\pm} & = & 80.4 \text{ GeV}/c^2 \\ p_\nu^x + p_{\bar{\nu}}^x & = & \not\!\!E_T^x \\ p_\nu^y + p_{\bar{\nu}}^y & = & \not\!\!E_T^y \end{array} \tag{8}$$

Because the two neutrinos escape the detector, the system is underconstrained for measuring the top mass. It becomes solvable by assuming a top mass independent distribution and using it as an additional constraint. In this analysis, the longitudinal momentum component of the $t\bar{t}$ system, $p_{t\bar{t}}^z$, was selected. The Monte Carlo simulations show that this variable is almost independent of the top mass and behaves according to a Gaussian distribution with a mean of zero and a width of 195 GeV/c. The validity of the Monte Carlo simulation was tested by using a sample of lepton+jets events. In that decay channel, $p_{t\bar{t}}^z$ can be explicitly reconstructed. In Fig. 9, the $p_{t\bar{t}}^z$ distribution obtained from a Monte Carlo simulation [25, 26] is compared with the observed distribution. The agreement is good and indicates that the Monte Carlo prediction of the $p_{t\bar{t}}^z$ distribution is on a sound basis.

Equations (8) can be combined into the following three relations:

$$\begin{array}{rcl} f_1(p_\nu^x, p_\nu^y, p_\nu^z) & \equiv & (E_{l^+} + E_\nu)^2 - (\vec{p}_{l^+} + \vec{p}_\nu)^2 - M_W^2 = 0 \\ f_2(p_\nu^x, p_\nu^y, p_\nu^z) & \equiv & (E_{l^-} + E_{\bar{\nu}})^2 - (\vec{p}_{l^-} + \vec{p}_{\bar{\nu}})^2 - M_W^2 = 0 \\ f_3(p_\nu^x, p_\nu^y, p_\nu^z) & \equiv & (E_{l^+} + E_\nu + E_b)^2 - (\vec{p}_{l^+} + \vec{p}_\nu + \vec{p}_b)^2 \\ & - & (E_{l^-} + E_{\bar{\nu}} + E_{\bar{b}})^2 + (\vec{p}_{l^-} + \vec{p}_{\bar{\nu}} + \vec{p}_{\bar{b}})^2 = 0. \end{array} \tag{9}$$

which become solvable when the momentum components of the second neutrino are expressed in terms of the transverse energy and momentum compnents of the first neutrino

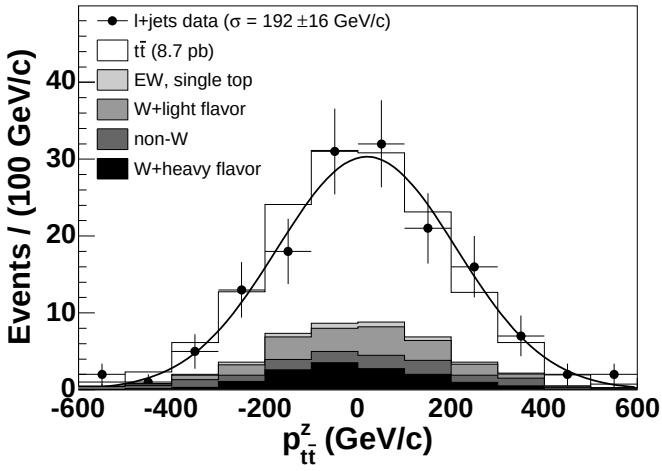

Figure 9: The $t\bar{t}$ longitudinal momentum component in the lepton+jets channel.

$$\begin{aligned} p_{\bar{\nu}}^x &= \not{E}_T^x - p_\nu^x \\ p_{\bar{\nu}}^y &= \not{E}_T^y - p_\nu^y \\ p_{\bar{\nu}}^z &= p_{t\bar{t}}^z - (p_b^z + p_{l^+}^z + p_\nu^z + p_{\bar{b}}^z + p_{l^-}^z). \end{aligned} \tag{10}$$

The neutrino three-momenta are obtained by solving Eqs. (9) and (10), thus yielding the top mass.

A wide range of possible $p_{t\bar{t}}^z$ values is incorporated by calculating the top mass 10000 times for each event. For each iteration, $p_{t\bar{t}}^z$ is drawn randomly from its expected distribution. Similarly, the jet energies and $\not{E}_T$ are smeared according to their resolutions. If a solution is not found with the above assumptions on M_W and M_t, these requirements are relaxed. The solutions within $M_{W^\pm} = 80.4 \pm 3.0$ GeV/c^2 and $M_t = M_{\bar{t}} \pm 2.0$ GeV/c^2 are accepted.

For a given event, two distributions are obtained for possible top-quark masses, each corresponding to a different lepton-jet pairing. The pairing that yields higher probability for finding a solution is selected. This choice is correct for 70% of simulated $t\bar{t}$ events. If the number of entries in this distribution is less than 100, the event is rejected. According to Monte Carlo studies, 91% of signal and 78% of background events pass this mass reconstruction requirement. The most probable value of a spline fit to the

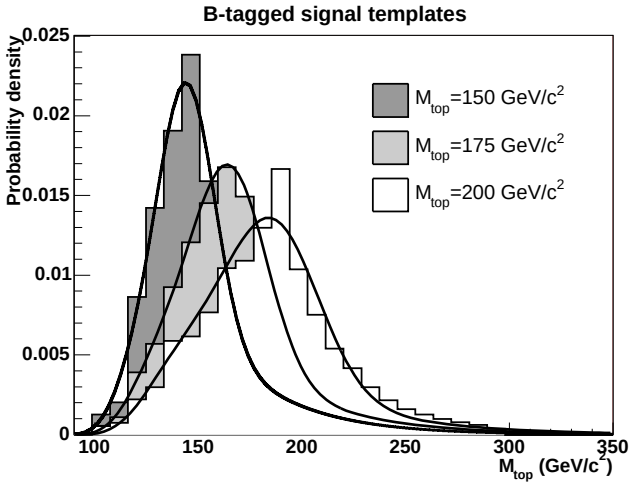

Figure 10: Signal templates for three different top masses. Overlaid functions are the signal template parametrizations at given masses.

selected distribution is taken as a per-event reconstructed top mass.

4.2.2 Signal and Background Templates

To model the expected reconstructed top mass distribution, templates were created from various simulated $t\bar{t}$ and background samples. Signal templates were generated from Monte Carlo simulation [25, 26] with top masses from 150 to 200 GeV/c^2 in 2 GeV/c^2 increments. After the templates were obtained, they were simultaneously parametrized to form continuos probability density functions f_s. The signal templates and probablity density functions were generated separately for b-tagged and non-tagged events. Examples of signal templates and functions f_s are shown in Fig. 10.

Background templates were generated for each background source, then combined according to the estimated yield of these. It was observed from simulation that using the same common background template for b-tagged and non-tagged samples provides as good a performance as using separate templates. The common background template, shown in Fig. 11, was therefore used for both subsamples.

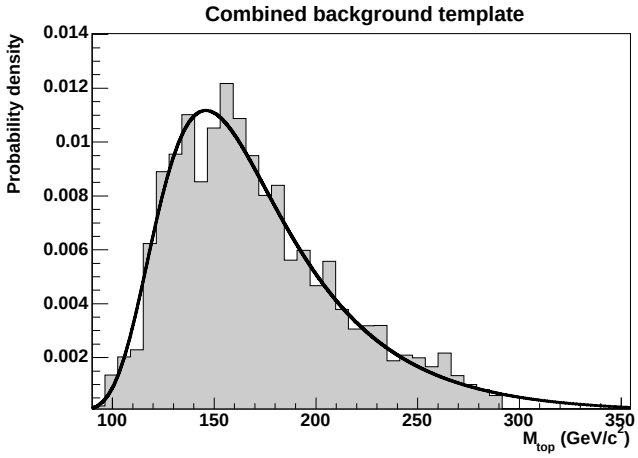

Figure 11: The combined background template together with the background template parametrization.

The final top mass estimate is extracted by comparing the reconstructed top mass distributions from data to the signal and background template parametrizations using an unbinned likelihood fit. The likelihood includes free parameters for the number of signal events ($n_{\rm s}^{\rm b}$ and $n_{\rm s}^{\rm non}$) and background events ($n_{\rm b}^{\rm b}$ and $n_{\rm b}^{\rm non}$) in each subsample, and for the top mass M_t. The total likelihood takes the form

$$\mathcal{L} \equiv \mathcal{L}_{\rm b-tagged}(M_t, n_{\rm s}^{\rm b}, n_{\rm b}^{\rm b}) \times \mathcal{L}_{\rm non-tagged}(M_t, n_{\rm s}^{\rm non}, n_{\rm b}^{\rm non}) \tag{11}$$

where each of the subsample likelihoods is:

$$\begin{aligned} \mathcal{L}_{\rm non/\mathit{b}-tagged} &\equiv \mathcal{L}_{\rm shape} \times \mathcal{L}_{\rm nev} \times \mathcal{L}_{\rm bg} \\ \mathcal{L}_{\rm shape} &\equiv \prod_{i=1}^{N} \frac{n_{\rm s} \times f_{\rm s}(m_{t_i}^{rec}, M_t) + n_{\rm b} \times f_{\rm b}(m_{t_i}^{rec})}{n_{\rm s}+n_{\rm b}} \\ \mathcal{L}_{\rm nev} &\equiv \frac{e^{-(n_{\rm s}+n_{\rm b})}(n_{\rm s}+n_{\rm b})^N}{N!} \\ -\ln \mathcal{L}_{\rm bg} &\equiv \frac{(n_{\rm b}-n_{\rm b}^{\rm exp})^2}{2\sigma_{n_{\rm b}}^2}. \end{aligned} \tag{12}$$

In the formula, N is the number of data events in the subsample, and $n_{\rm b}^{\rm exp}$ and $\sigma_{n_{\rm b}}$ are the expected number of background events and its uncertainty.

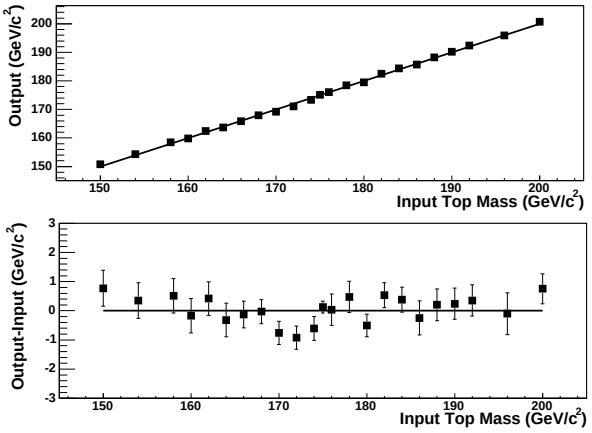

Figure 12: Summary of simulated experiments. The upper plot shows the mean of the output top mass as a function of the generated top mass, the lower plot shows the difference between the output and generated top masses as a function of the generated top mass.

The top-quark mass hypothesis which minimizes -ln($\mathcal{L}$) is taken.

4.2.3 Simulated experiments

To validate the method, simulated experiments were carried out. In the simulated experiments, a set of events is randomly selected from a sample of Monte Carlo events, and the top mass estimate is calculated by using a likelihood fit. This procedure is repeated 10000 times. For each repetition, a top mass estimate and its statistical uncertainty is obtained, and the mass estimate is compared to the generated input top mass. Figure 12 shows a summary of the comparisons between output and input masses. Since the top mass estimates are consistent with the generated top masses, we conclude that the method is unbiased.

In order to check the consistency between the spread in the output top masses and the estimated statistical uncertainty (σ), pull distributions are generated:

$$\text{pull} \equiv \frac{M_{\text{out}} - M_{\text{in}}}{\sigma} \tag{13}$$

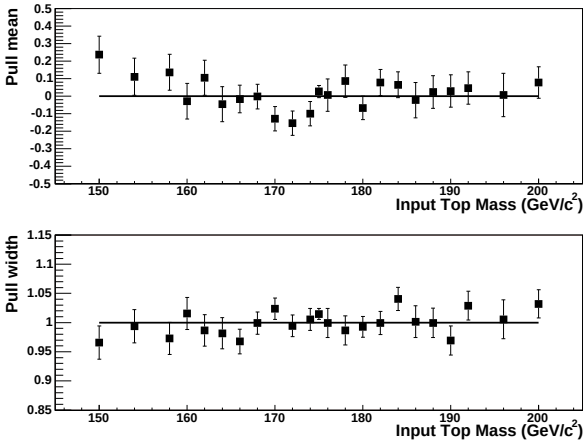

Figure 13: Summary of pull distributions. The upper plot shows the pull means as a function of the generated top mass, the lower plot shows the pull widths as a function of the generated top mass.

A summary of the pull studies is shown in Fig. 13. Unity pull widths indicate that the statistical uncertainties are estimated correctly.

4.2.4 Final Top Mass Estimate from Data

The measurement from the data is performed with a sample corresponding to 1.2 fb^{-1}. This sample contains 77 events passing the event selection, out of which 70 events pass the mass reconstruction requirement. Of the 70 events, 33 are b-tagged and 37 are non-tagged. The final top mass estimate is calculated using the likelihood fit described in Eq. (11). The result from the likelihood fit is

$$M_t = 169.7^{+5.2}_{-4.9}(\text{stat})\ \text{GeV}/c^2. \tag{14}$$

The reconstructed top mass distribution together with the signal and background parametrizations are shown in Fig. 14.

The measurement from the data sample corresponding to 0.34 fb^{-1} utilizes similar method as the method described in this section. The details are fully described in Publication I. The top mass estimate from this data

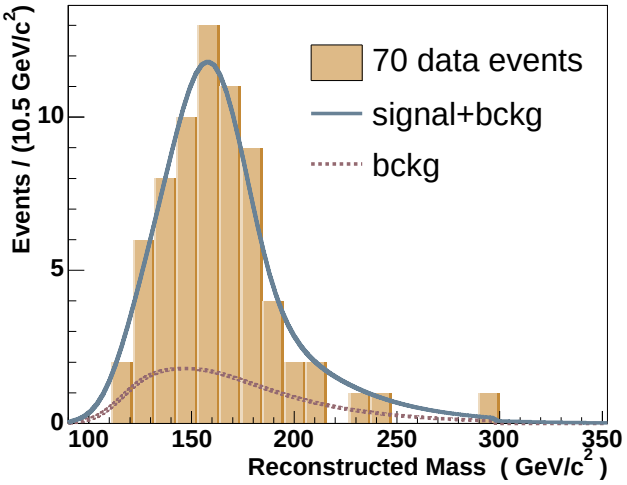

Figure 14: The reconstructed top mass distribution from data together with the signal + background (M_t = 169.7 GeV/c^2) and the background parametrization functions.

sample is

$$M_t = 169.5^{+7.7}_{-7.2}(\text{stat}) \pm 4.0(\text{syst})\ \text{GeV}/c^2. \tag{15}$$

4.3 Cross-Section-Constrained Mass Measurement

The template top mass measurement can be further improved by taking into account the top mass dependence of the $t\bar{t}$ production cross section. In this measurement, the top mass information is extracted from the reconstructed top mass distribution as well as the observed number of events. The per-event mass reconstruction method and template parametrizations are exactly the same as in the template top mass measurement described in Chapter 4.2. The likelihood function is a modified version of Eq. (11): the number of signal events is not a free fit parameter, but it is expressed as a function of the top mass, $n_s(M_t)$.

The expected number of signal events can be expressed as

$$n(M_t) = \sigma_{t\bar{t}}(M_t) \cdot a(M_t) \cdot \mathcal{L} \cdot p^{rec}_{mass}, \tag{16}$$

where $\sigma_{t\bar{t}}(M_t)$ is the theoretical $t\bar{t}$ cross section, $a(M_t)$ is the acceptance of $t\bar{t}$ events, $\mathcal{L}$ is the integrated luminosity, and p^{rec}_{mass} is the mass reconstruction probability.

The dominant top mass dependence on the expected number of events comes from the theoretical $\sigma_{t\bar{t}}$. We use a NLO theoretical calculation of $\sigma_{t\bar{t}}$ evaluated at three different top masses [10], and parametrize the mass dependence of $\sigma_{t\bar{t}}$ on the top mass using the functional form described in [8]:

$$\sigma_{t\bar{t}}(M_t) = 6.70 \cdot e^{(175-M_t)/32.29} \text{ pb}. \tag{17}$$

The acceptance $a(M_t)$ was studied from a Monte Carlo simulation and corrected for known differences between the data and simulation. The CDF integrated luminosity was measured with Cherenkov luminosity counters [27]. The mass reconstruction probability was studied from the Monte Carlo simulation.

Simulated experiments proved that the cross-section-constrained method is unbiased and returns appropriate errors. From a data sample of 1.2 fb^{-1}, we measure a top mass of

$$M_t = 170.7^{+4.2}_{-3.9}(\text{stat}) \text{ GeV}/c^2. \tag{18}$$

Figure 15 shows the cross-section-constrained top mass measurement in the M_t – $\sigma_{t\bar{t}}$ plane.

4.4 Systematic Uncertainties

Systematic uncertainties arise from uncertainties in the Monte Carlo simulation, detector response, and various assumptions made during implementation of the mass measurement technique. The magnitudes of such uncertainties were estimated by adjusting the kinematics of the input events, number of events, or both at the same time in simulated experiments. The resulting mean top mass was compared to the nominal result.

The measured energy of jets is calibrated using simulated and data events. Due to lack of knowledge of the underlying processes in hadronization and limited data statistics, there is an uncertainty in the correction of the raw jet energy [28]. The systematic uncertainty on the top mass was studied

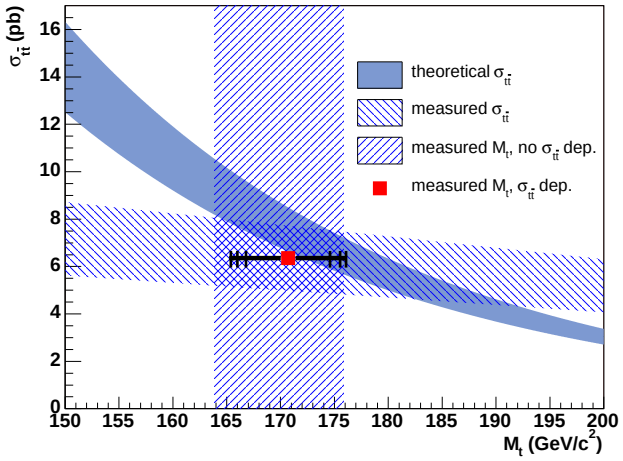

Figure 15: The measured cross-section-constrained top mass shown in M_t – $\sigma_{t\bar{t}}$ plane. The innermost error bars correspond to the statistical uncertainty, the middle ones statistical+systematic uncertainty, and the outermost error bars show statistical+systematic+theory uncertainty. The hatched areas mark the template top mass measurement without the cross-section-constraint and the $\sigma_{t\bar{t}}$ measurement in the dilepton channel. The theoretical $\sigma_{t\bar{t}}$ is marked with the solid-colored band.

by varying the jet energies by one unit of uncertainty in the response, and measuring the difference in the extracted top masses. Since the nominal jet corrections are determined for light quark jets, additional uncertainty was estimated to account for possible differences between light quark and b-jets [29].

The signal modeling uncertainty takes into account differences in parton showering between the PYTHIA [25] and HERWIG [30] Monte Carlo generators, uncertainties in initial and final state radiation modeling, and differences in parton distribution functions between MRST [31] and the full set of CTEQ6M [32] eigenvectors. Possible imperfections in the modeling the $Z \rightarrow ll$ and fake lepton backgrounds are included in the background modeling uncertainty. The uncertainties from template statistics as well as from lepton p_T were also estimated.

The cross-section-constrained measurement has an additional systematic uncertainty from the expected number of events. This uncertainty includes uncertainties in the integrated luminosity, the acceptance, the expected number of background events (including relative background composition), and the mass reconstruction probability.

All the sources of uncertainty and their magnitudes are summarized in Table 3. The total systematic uncertainty on the pure template top mass measurement is 3.1 GeV/c^2 and on the cross-section-constrained measurement 2.6 GeV/c^2.

Table 3: Summary of systematic uncertainties for the pure template (T) and the cross-section-constrained (C) measurement. The uncertainties were combined in quadrature.

Systematic Source	ΔM_t (GeV/c^2)	
	T	C
Jet energy scale	2.9	1.8
Signal modeling	0.8	0.9
Background modeling	0.3	0.3
Background composition	0.3	n.a
Template statistics	0.5	0.4
Lepton p_T	0.2	0.2
Expected number of events	n.a	1.6
Total	3.1	2.6

The probability shape of the theoretical $\sigma_{t\bar{t}}$ uncertainty is not well understood. We performed several studies to estimate the effect of this theoretical uncertainty on the top mass determination. It was concluded that the uncertainty on the top mass is not very sensitive to the probability shape of the theoretical $\sigma_{t\bar{t}}$ uncertainty. Thus, the simplest way to calculate the uncertainty on the top mass was selected: in simulated experiments, the numbers of signal events were changed according to the theoretical uncertainty of $^{+0.71}_{-0.88}$ pb [10]. The resulting uncertainty due to theory on the cross-section-constrained top mass measurement is 2.4 GeV/c^2.

4.5 Comparison to Other Top-Quark Mass Measurements

The CDF Collaboration has measured the top-quark mass in the dilepton [33], lepton+jets [34, 35, 36], and all-hadronic [37, 38] channels with complementary methods in each channel, and the DØ Collaboration has measured it in the dilepton [39, 40] and lepton+jets [41, 42] channels with complementary methods. In Fig. 16, the most precise measurements from each channel using data sets corresponding to 1.0–1.2 fb^{-1} are compared to the measurements described in this thesis. All three measurements described in this thesis are in good agreement with each other, with other measurements in the dilepton channel, and with top-quark mass measurements in the lepton+jets and all-hadronic channels. The cross-section-constrained measurement provides the single most precise top-quark mass measurement in the dilepton channel in this data sample.

The current world average of experimental top-quark mass measurements gives $M_t = 170.9 \pm 1.1(\text{stat.}) \pm 1.5(\text{syst.})$ GeV/c^2. The average is consistent with the indirect top-quark mass achieved from electroweak fits, $M_t = 178^{+12}_{-9}$ GeV/c^2 [17]. This agreement builds confidence that the electroweak fits provide trustworthy predictions of the SM Higgs-boson mass. With 95% C.L., the electroweak fits predict the Higgs-boson mass to be $M_H < 144$ GeV/c^2 [17]. It complements the direct limit from LEP Higgs searches, $M_H > 114$ GeV/c^2 with 95% C.L. [43].

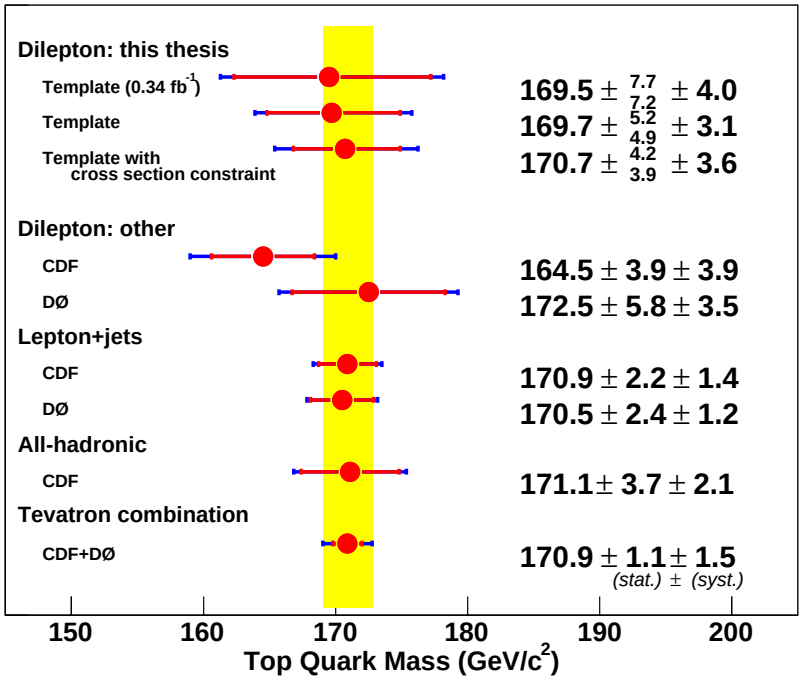

Figure 16: Summary of experimental measurements of the top-quark mass. These measurements use data sets corresponding to 1.0–1.2 fb^{-1}, and only the most precise in each category is shown.

5 Summary

The top-quark mass measurement is currently one of the most important measurements in experimental particle physics. For example, the top mass places constraints in the SM Higgs-boson mass.

This thesis describes three top-quark mass measurements in the dilepton channel. In these analyses, the underconstrained system in the dilepton channel is solved using a top mass independent distribution of $p_{t\bar{t}}^{z}$, and a reconstructed top mass is calculated for each event. The final top mass estimate is achieved by comparing the reconstructed top mass distribution to template distributions. In the cross-section-constrained measurement, comparison of the observed number of events with theoretical expectations was

used to further constrain the top mass measurement.

With 0.34 fb^{-1} of data, the template measurement results in a top-quark mass of $169.5^{+7.7}_{-7.2}(\text{stat}) \pm 4.0(\text{syst})$ GeV/c^2. The method was improved by dividing the sample into b-tagged and non-tagged subsamples. From a data sample of 1.2 fb^{-1}, the enhanced template measurement gives a top-quark mass of $169.7^{+5.2}_{-4.9}(\text{stat}) \pm 3.1(\text{syst})$ GeV/c^2.

The third result takes into account the top mass dependence of the expected number of events. From a data sample of 1.2 fb^{-1}, we measure a top-quark mass of $170.7^{+4.2}_{-3.9}(\text{stat}) \pm 2.6(\text{syst}) \pm 2.4(\text{theory})$ GeV/c^2. This result is the single most precise measurement of the top-quark mass in the dilepton channel in this data sample. All three measurements are consistent with each other and with other top-quark mass measurements.

References

[1] See for example: F. Haltzen and A. Martin, *Quarks and Leptons: An Introductory Course in Modern Particle Physics* (John Wiley & Sons, 1984).

[2] F. Abe *et al.* (The CDF Collaboration), Phys. Rev. Lett. **74**, 2626 (1995).

[3] S. Abachi *et al.* (The DØ Collaboration), Phys. Rev. Lett. **74**, 2632 (1995).

[4] S. Herb *et al.* Phys. Rev. Lett. **39**, 252 (1977).

[5] W. R. Innes *et al.* Phys. Rev. Lett. **39**, 1240 (1977).

[6] The Tevatron Electroweak Working Group (CDF and DØ Collaborations), hep-ex/0703034.

[7] S. Willenbrock, The Standard Model and the Top Quark, Lectures presented at the Advanced Study Institute on Techniques and Concepts of High Energy Physics, St. Croix, U. S. Virgin Islands, June 13-24, 2002, hep-ph/0211067 (2002).

[8] S. Catani *et al.*, Phys. Lett. B **378**, 329 (1996).

[9] On-line plotting and calculation of PDFs, http://durpdg.dur.ac.uk/hepdata/pdf3.html

[10] M. Cacciari *et al.*, J. High Energy Phys. **04**, 68 (2004).

[11] B. W. Harris *et al.*, Phys. Rev. D **66**, 054024 (2002).

[12] Z. Sullivan, Phys. Rev. D **70**, 114012 (2004).

[13] V. M. Abazov *et al.* (DØ Collaboration), Phys. Rev. Lett. **98**, 181802 (2007).

[14] F. Abe *et al.* (The CDF Collaboration), Phys. Rev. D **50**, 5550 (1994).

[15] I.I. Bigi *et al.*, Phys. Lett. B **181**, 157 (1986).

[16] W.-M. Yao *et al.* (Particle Data Group), J. Phys. G Nucl. Part. Phys. **33**, 1 (2006).

[17] The LEP Collaborations, LEP Electroweak Working Group, SLD Electroweak and Heavy Flavor Groups, CERN-PH-EP/2007-039.

[18] C. T. Hill, Phys. Lett. B **345**, 483 (1995).

[19] A. Delgado and T.M.P. Tait, J. High Energy Phys. **07**, 23 (2005).

[20] G. L. Kane and S. Mrenna, Phys. Rev. Lett. **77**, 3502 (1996).

[21] T. Sjostrand and V.A. Khoze, Phys. Rev. Lett. **72**, 28 (1994).

[22] CDF II Technical Design Report, Fermilab-Pub-96/390-E (1996).

[23] D. Acosta *et al.* (CDF Collaboration), Phys. Rev. D **71**, 032001 (2005).

[24] D. Acosta *et al.* (CDF Collaboration), Phys. Rev. Lett. **93**, 142001 (2004).

[25] T. Sjostrand *et al.*, Comput. Phys. Commun. **135**, 238 (2001).

[26] T. Affolder *et al.*, Nucl. Instrum. Methods Phys. Res. A**447**, 1 (2000).

[27] D. Acosta *et al.*, Nucl. Instrum. Methods A**494**, 57 (2002).

[28] A. Bhatti *et al.*, Nucl. Instrum. Methods A**566**, 375 (2006).

[29] A. Abulencia *et al.* (CDF Collaboration), Phys. Rev. D **73**, 032003 (2006).

[30] G. Corcella *et al.*, J. High Energy Phys. **01**, 10 (2001).

[31] A. D. Martin *et al.*, Phys. Lett. B **356**, 89 (1995).

[32] J. Pumplin *et al.*, J. High Energy Phys. **0207**, 012 (2002).

[33] A. Abulencia *et al.* (CDF Collaboration), Phys. Rev. D **75**, 031105 (2007).

[34] T. Aaltonen *et al.* (CDF Collaboration), Phys. Rev. Lett. **99**, 182002 (2007).

[35] T. Aaltonen *et al.* (CDF Collaboration), CDF public note 8780.

[36] T. Aaltonen *et al.* (CDF Collaboration), CDF public note 8669.

[37] T. Aaltonen *et al.* (CDF Collaboration), Phys. Rev. D **76**, 072009 (2007).

[38] T. Aaltonen *et al.* (CDF Collaboration), CDF public note 8709.

[39] V. M. Abazov *et al.* (DØ Collaboration), DØ public note 5463.

[40] V. M. Abazov *et al.* (DØ Collaboration), DØ public note 5347.

[41] V. M. Abazov *et al.* (DØ Collaboration), DØ public note 5362.

[42] V. M. Abazov *et al.* (DØ Collaboration), DØ public note 4728.

[43] ALEPH, DELPHI, L3, and OPAL Collaborations, Phys. Lett B **565**, 61 (2003).